# Dynamics in Polymer−Silicate Nanocomposites As Studied by Dielectric Relaxation Spectroscopy and Dynamic Mechanical Spectroscopy

**Jovan Mijović,*,† HyungKi Lee,† Jose Kenny,‡ and Jimmy Mays§**

*Othmer Department of Chemical and Biological Engineering, Polytechnic University, Six Metrotech Center, Brooklyn, New York 11201; Department of Materials Science and Technology, University of Perugia, 05100 Terni, Italy; and Department of Chemistry, University of Tennessee, Knoxville, Tennessee 37996*

*Received September 13, 2005; Revised Manuscript Received January 21, 2006*

ABSTRACT: Nanocomposites of organically modified clay nanoparticles and a polyisoprene (PI) matrix were prepared by solution-mediated intercalation, and their dynamics were investigated over a broad range of frequency and temperature by dielectric relaxation spectroscopy (DRS) and dynamic mechanical spectroscopy (DMS). The principal goal was to address the effect of geometric confinement and elucidate how the dynamics vary as a function of the type and concentration of clay and the molecular weight of PI. Dielectric spectra of nanocomposites with low-molecular-weight PI reveal no effect of clay loading on the average relaxation time for segmental and normal mode relaxation, but dc conductivity and interfacial polarization are affected. In nanocomposites with high molecular weight PI (in the entangled regime), however, a clear effect of clay loading on the average relaxation time for the normal mode process is observed. Most interestingly, it is found that the normal mode becomes faster with increasing clay content, and an explanation is offered in terms of the preferential suppression of the longer scale (lower frequency) portion of the normal mode spectrum. The average relaxation times for segmental and normal mode calculated from dielectric and viscoelastic measurements are in excellent agreement. DMS measurements also reveal an increase in the magnitude of storage and loss modulus with increasing clay loading up to the threshold value of 8 wt %. The observed increase originates from the "filler effect".

## Introduction

Nanocomposites consisting of layered-silicate nanoparticles in a polymer matrix have attracted considerable technological and scientific interests in recent years due to their outstanding physical and mechanical properties, such as high strength and stiffness, flame retardation, and gas permeability barrier.[1−3] The key attraction here is that the desired materials' properties and functions are obtained *not* by manipulating the structure at the atomic or molecular level, where much of the existing chemical knowledge lies, *but* by designing nanoscopic building blocks that offer new and unique properties. But in order to realize the macroscopic properties of nanocomposites from molecular concepts, one must understand the molecular motions, or dynamics, of these materials in response to various applied fields.

When placed in an electric field, for example, nanocomposites are subject to ionic, interfacial, and dipole polarization. Those polarization mechanisms have considerably different time scales and length scales, making dielectric spectroscopy, with its unparalleled range of frequency and temperature, uniquely suited for the study of nanocomposite dynamics.

Nanocomposites investigated herein are composed of nanoparticles of organically modified clay and *cis*-polyisoprene matrix. Organic modification improves compatibility and dispersion of nanoparticles in the nonpolar matrix. The use of *cis*-polyisoprene (PI) as matrix adds another important dimension to the study of dynamics of these nanocomposites by dielectric relaxation spectroscopy. PI chains exhibit, in addition to the transverse dipole moment that gives rise to the segmental process, a persistent cumulative dipole moment along the chain contour that may be relaxed via the normal mode process.[4−6] For a sequence of repeat units in the PI chain (without reversal of directional sense), the dipole vector must correlate with the displacement vector, implying correspondence between dielectric and low-frequency viscoelastic measurements. This is an important point because those two techniques average chain motions differently,[7] yet when combined judiciously they are conducive to addressing a number of critical dynamics issues such as the spectral broadening, the spatial heterogeneity, the distribution of relaxation times, and so on. Furthermore, segmental and normal mode motions in geometrically confined PI chains may show different relaxation behavior from the bulk.

Good dispersion of nanoparticles in the polymer matrix is the key requirement for attaining superior properties in nanocomposites, and there have been contradicting reports about the miscibility of PI with layered silicates. For example, in one such study PI and nanoclay were termed immiscible because their nanocomposites did not show a measurable change in the gallery spacing.[8] But Jeon et al. reported improved rheological properties with increasing clay loading,[1,9] which they attributed to the exfoliation of different silicate layers in the PI matrix. Vu et al. utilized X-ray diffraction and also reported intercalation and exfoliation of organically modified clay in 1,4-*cis*-polyisoprene rubber (ENR)/silicate nanocomposites.[10] At present, however, it is fair to say that the diffusion of PI into silicate galleries remains incompletely understood. Moreover, most studies of PI−silicate nanocomposites have focused on the effect of intercalated or exfoliated clay on the physical/mechanical properties in the *bulk*, while less attention has been paid to the underlying physics on the *molecular level*.

* To whom correspondence should be addressed. E-mail: jmijovic@poly.edu.
† Polytechnic University.
‡ University of Perugia.
§ University of Tennessee.

10.1021/ma051995e CCC: $33.50 
Published on Web 02/21/2006

**Table 1. Sample Description and Codes**

| description | $M_w$ (g mol$^{-1}$) | $M_w/M_n$ | code | clay weight (%) |
|---|---|---|---|---|
| *cis*-1,4 polyisoprene | 2770 | 1.05 | Pl3 | |
| *cis*-1,4 polyisoprene | 26900 | 1.07 | Pl30 | |
| composites: Pl3 + Cloisite 25A | | | Pl3C25A | varies |
| composites: Pl3 + Cloisite 30B | | | Pl3C30B | varies |
| composites: Pl30 + Cloisite 25A | | | Pl30C25A | varies |
| composites: Pl30 + Cloisite 30B | | | Pl30C30B | varies |

The combined use of dielectric relaxation spectroscopy (DRS) and dynamic mechanical spectroscopy (DMS) aimed at probing the dynamics of PI−silicate nanocomposites has not been systematically explored. The principal objective of this study is to establish the effect of the type and concentration of clay on the time scale and length scale of various relaxation processes as measured by dielectric and viscoelastic techniques.

## Experimental Section

**Materials.** Commercial *cis*-polyisoprene (PI3) with number-average molecular weight ($M_n$ = 2770 g/mol) was purchased from Polysciences Inc. Another polyisoprene sample (PI30) of higher molecular weight ($M_n$ = 26 900 g/mol), used as a reference, was synthesized by anionic polymerization.[11] To improve miscibility of layered silicates with polymers, the hydrophilic silicate surface is converted to an organophilic one through ion-exchange reactions with alkylammonium cations, resulting in lower surface energy and improved wetting. Two organically modified clays (Cloisite 25A and 30B), with the cation-exchange capacity (CEC) of 90 mequiv/100 g, were supplied by Southern Clay Products, Inc., and were used as fillers without further purification. The organic modifiers used include dimethyl hydrogenated-tallow-2-ethylhexyl (2MHTL8) and methyl-tallow-bis(2-hydroxyethyl) (MT2EtOH) quaternary ammonium. Table 1 summarizes the samples investigated and specifies their codes.

**Dielectric Relaxation Spectroscopy (DRS).** In DRS measurements, the real and imaginary dielectric permittivity were determined as a function of frequency ($10^{-1}$−$10^6$ Hz) in the temperature range from −50 to 50 °C (controlled to better than ±0.1 °C). A Novocontrol α analyzer (3 $\mu$Hz−10 MHz) was used. The instrument is interfaced with computer and equipped with a custom-modified Novocool heating and cooling system for sequential measurements from low to high frequency.

**Dynamic Mechanical Spectroscopy (DMS).** Rheological measurements were performed on a Rheometrics Scientific ARES rheometer in the frequency range from 0.1 to 100 rad/s with temperature control (−60 to 30 °C) in order to generate dynamic storage and loss modulus in the frequency domain. To determine the limits of linear viscoelastic properties of PI3, PI3C30B, and PI3C25A (see Table 1 for sample codes), dynamic strain sweeps were performed in the controlled strain rate mode using parallel plate geometry (8 mm diameter plates). The gap was set in the range from 1 to 1.5 mm.

**Characterization.** Low-angle X-ray diffraction measurements were performed using an X-ray detector (Scintag XI diffractometer) to estimate gallery separation in the layered silicates. The measurements were started from the diffraction angle $2\theta = 2°$ up to 8° at a rate of 1°/min. The shift between the intensity peaks in organically modified clay and PI−silicate nanocomposites was measured within the available range of diffraction angle of our instrument.

**Preparation of Nanocomposites.** PI−silicate nanocomposites were prepared by solution mixing of monodisperse PI and organically modified clay in toluene at room temperature and by stirring vigorously for 15 h. The resulting solution has the characteristics of a colloidal suspension because the layered silicates retain their crystal platelet structure during shear blending. The homogeneous solution was dried at 35 °C in a vacuum oven for 3 days, until the remaining solvent was completely removed.

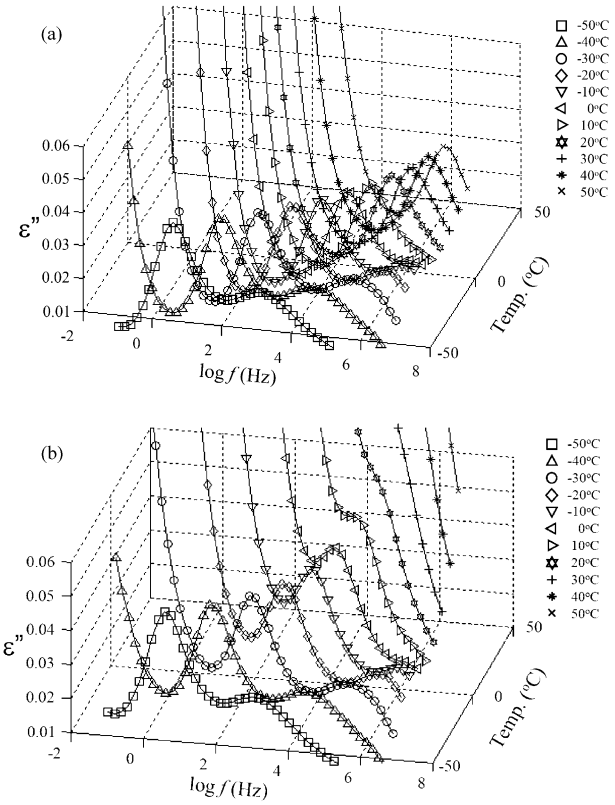


**Figure 1.** Dielectric loss as a function of frequency and temperature for (a) 1,4-*cis*-polyisoprene (PI) ($M_n$ = 2770 g/mol, $M_w/M_n$ = 1.05) and (b) PI3C25A(5%).

## Results and Discussion

**Neat Polyisoprene.** The background on dielectric properties of polymers and the principal features of the dynamics in glass-formers have been described in great detail in a number of books and key reviews[12−16] and will not be reviewed here. We begin by briefly examining the dielectric response of neat polyisoprene (PI). Since the DRS studies of neat PIs have been reported by several groups,[4−6,17] our goal here is not to be comprehensive. Dielectric loss as a function of frequency and temperature (between −50 and 50 °C, at 10 °C intervals) for PI3 is shown in Figure 1a. Normal ($\alpha_N$) and segmental ($\alpha_S$) relaxation processes are readily discernible in the loss spectra and exhibit the usual Vogel−Fulcher−Tammann (VFT) temperature dependence of the average relaxation time. Analogous results were obtained for the higher molecular weight PI30. The solid lines in Figure 1a are combined fits to the sum of the ionic conductivity term and the Havriliak−Negami (HN) functional forms for normal and segmental relaxation modes. Note that the distance between the two peaks ($\alpha_N$ and $\alpha_S$) varies little within the temperature range used in this study, while conductivity dominates the low-frequency tail of the spectrum.

**Nanocomposites.** We start by showing dielectric loss as a function of frequency and temperature for PI3C25A(5%). The spectra shown in Figure 1b were also obtained in the temperature range between −50 and 50 °C, at 10 °C intervals. Normal ($\alpha_N$) and segmental ($\alpha_S$) relaxation processes are present and are well described by the HN fits. The most apparent difference between the neat PI3 and the PI3C25A(5%) nanocomposite is at the low-frequency end of the spectrum. Note how conductivity encroaches onto the normal mode much faster in PI3C25A(5%)

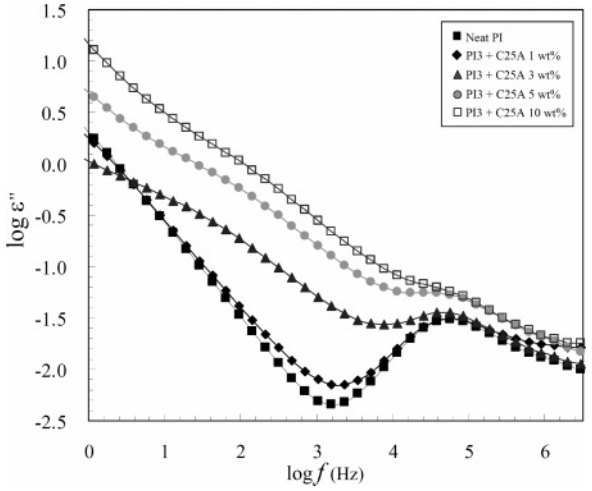


**Figure 2.** Dielectric loss in the frequency domain for PI3 and its nanocomposites with clay loading as a parameter at $T = 283$ K.

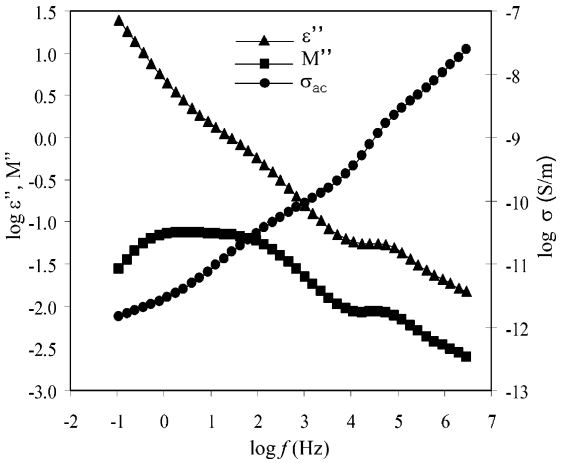


**Figure 3.** Maxwell−Wagner−Sillars and normal mode relaxation for PI3C25A(5%) in the frequency domain expressed in three different formalisms: dielectric loss, dielectric loss modulus, and ac conductivity at $T = 283$ K.

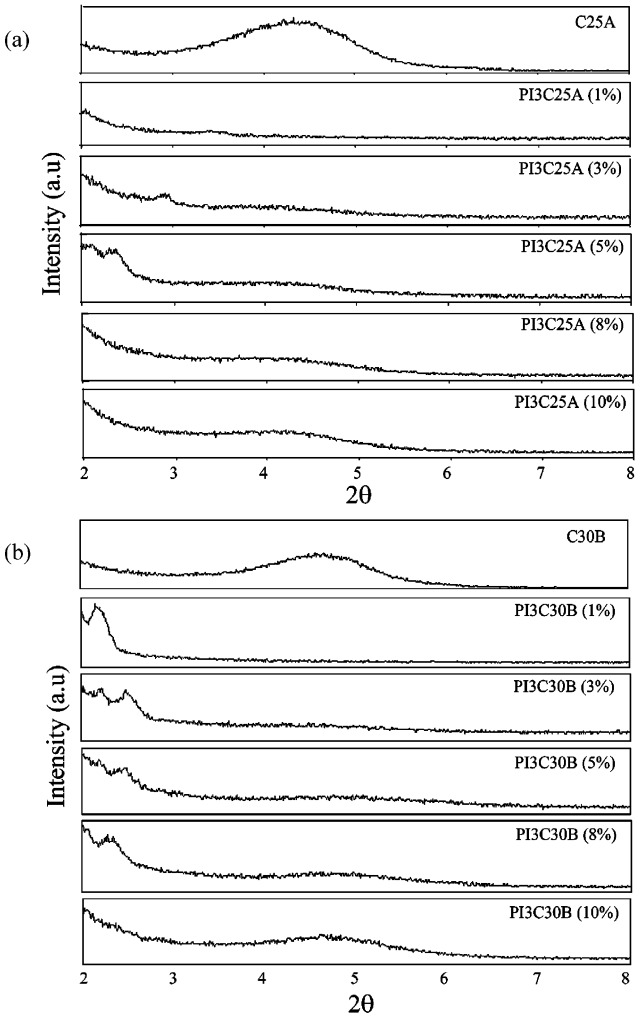


**Figure 4.** X-ray diffraction patterns of (a) PI3C25A and (b) PI3C30B nanocomposites with clay loading as a parameter.

than in the neat PI3 and how this effect becomes more pronounced with increasing temperature.

We next take a closer look at the frequency region dominated by conductivity and examine the effect of clay loading on the dielectric response. Figure 2 shows dielectric loss in the frequency domain at 283 K, with clay loading percentage as a parameter. At that temperature, the normal mode process is visible at the high-frequency end of the spectrum. Two salient points characterize the spectra of Figure 2. First, we note that the conductivity increases with increasing clay loading from 1 to 10%. And second, at loadings of 3% and higher, the shape of the low-frequency end of the dielectric loss spectrum changes, and we observe a gradual development of a shoulder in the range between 10 and $10^3$ Hz. The emergence of this shoulder is the manifestation of the evolvement of the Maxwell−Wagner−Sillars (MWS) or interfacial polarization. MWS polarization is a characteristic of heterogeneous systems and is caused by charges blocked at the internal phase boundaries.[18−21]

In systems like ours, where dielectric response encompasses contributions from conductivity, interfacial polarization (MWS), and segmental and normal mode dipolar relaxations, it is often advantageous to resort to different representations of data in order to suppress or enhance a particular process.[22] To that end, Figure 3 shows the results for a sample of PI3C25A(5%) measured at 283 K and plotted using three different formalisms: dielectric loss, dielectric modulus, and conductivity. The MWS polarization is manifest in all three formalisms; it appears as a shoulder in the dielectric loss spectrum, a part of a broad peak in the dielectric modulus spectrum, and a shoulder in the conductivity spectrum. In the modulus representation, conductivity and the MWS polarization overlap and give rise to a broad peak. In the low-frequency range, conductivity approaches the frequency-independent dc value. Throughout the text, we shall resort to different formalisms in attempts to best describe and interpret the effect of heterogeneity on the dielectric response of nanocomposites.

Before proceeding with the quantitative analysis of the dielectric spectra, we briefly examine the extent of intercalation and/or exfoliation that takes place as a result of polymer percolation into the gallery of silicate layers. Among experimental techniques, X-ray diffraction (XRD) is particularly useful in determining the basal spacing between the clay platelets. The changes in the XRD pattern of intercalated PI3C25A and PI3C30B as a function of clay loading are shown in Figure 4a,b for the diffraction angle ($2\theta$) in the range between 2° and 8°. The two types of neat clay have different peaks; for C25A $2\theta = 4.21°$ (Figure 4a) and for C30B $2\theta = 4.68°$ (Figure 4b). Those initial peaks remain at their respective locations but decrease in intensity with decreasing amount of clay. Simultaneously, a new peak due to the intercalation of layered silicates appears and shifts to lower diffraction angle with increasing clay loading. The intercalated structure of different basal spacing varies with

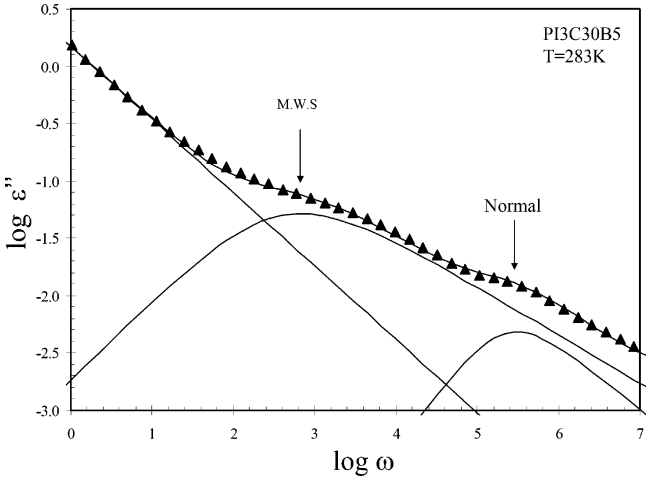


**Figure 5.** Dielectric loss in the frequency domain for PI3C30B (5%) at $T = 283$ K. The spectrum was deconvoluted into the Maxwell−Wagner−Sillars and normal mode relaxation.

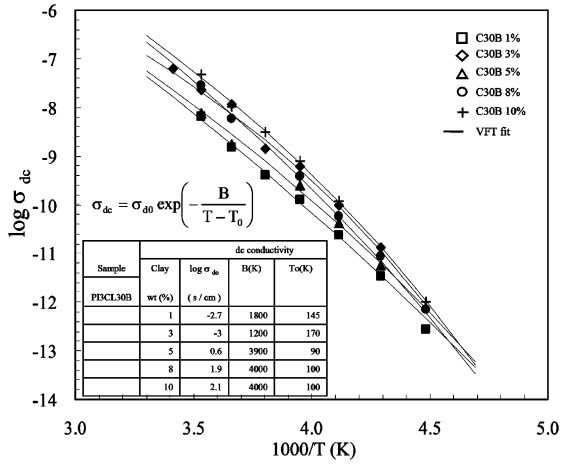


**Figure 6.** Conductivity as a function of reciprocal temperature for PI3C30B nanocomposites with different clay loading. Solid lines are fits to the VFT functional form.

the amount and the type of clay. For example, a comparison of the XRD spectra of PI3C25A and PI3C30B reveals that the latter have well-ordered intercalated structure, while the former are more intercalated/exfoliated, as indicated by the sharper Bragg peaks in Figure 4b.[23] PI3C25A(1%) appears mostly exfoliated with a small intercalation peak at around $2\theta = 3.4°$.

We next proceeded to quantify the spectra by fitting the dielectric loss data in the frequency domain as a function of composition and temperature. As illustrated in Figure 5, deconvolution of the loss spectrum at 283 K gives rise to (1) the peak at higher frequency due to the normal mode process ($\alpha_N$), (2) the larger and broader peak at lower frequency due to the MWS polarization ($\alpha_{MWS}$), and (3) the conductivity contribution at lower frequencies ($\sigma$).[3] The analysis was performed using the following expression that combines the conductivity term with the HN functional form for each relaxation process.[24,25]

$$\epsilon^* = -i\frac{\sigma_{dc}}{\epsilon_0 \omega^s} + \epsilon_\infty + \sum_j \frac{(\Delta\epsilon)_j}{[1 + (i\omega\tau_j)^\alpha]^\beta} \qquad (1)$$

where $\sigma_{dc}$ is the dc conductivity, $\omega$ is the angular frequency, $s$ is an exponent ($0 < s \leq 1$), $\tau_j$ is the relaxation time of the $j$th process, $\epsilon_0$ is the vacuum permittivity, $\Delta\epsilon$ is the dielectric strength of the $j$th process, and $\alpha$ and $\beta$ are the shape parameters of the HN function that define the breadth and the symmetry of the spectrum. The results for PI3C30B and PI3C25A were analyzed and are recapped below for each polarization mechanism.

**Conductivity/Charge Migration.** In general, conductivity ($\sigma$) may be described by a frequency-independent part, $\sigma_{dc}$, associated with the migration of unbound charges, and a frequency-dependent part, $\sigma_r$, associated with relaxation. The temperature dependence of $\sigma_{dc}$ is shown in Figure 6. In the inset in Figure 6 we list the fit parameters obtained from the analysis of the normal mode process (eq 1) and the VFT equation as follows:[12,18,26,27]

$$\sigma_{dc} = \sigma_{d0} \exp\left(-\frac{B}{T - T_0}\right) \qquad (2)$$

where $\sigma_{d0}$, $B$, and $T_0$ (Vogel temperature) are temperature-independent constants that are fitted to the conductivity data obtained from eq 1. As shown in Figure 6, the fits are excellent, and the temperature dependence of $\sigma_{dc}$ is well described by the VFT form, suggesting that the conductivity is governed by the motions of PI chains. Conductivity lines for various clay loadings run parallel to each other over a wide range of temperature and get closer only as the $T_g$ is approached. As shown in the table (inset) in Figure 6, the fit parameters $B$ and $T_0$ appear to reach a threshold value beyond which there is no further effect of clay loading on conductivity.

**Segmental and Normal Mode Dipolar Relaxation.** Insertion of PI chains between intercalated or exfoliated clay platelets raises the question of how the restricted space, or confinement, affects the segmental and normal mode processes. The effect of confinement on the dynamics of glass formers is an important issue in condensed matter physics and is currently the subject of considerable experimental, theoretical, and computational work.[28−30] Following the work of Jackson and McKenna on the effect of confinement on glass transition,[31,32] a number of studies have been published reporting an increase, decrease, or no change in dynamics as expressed by $T_g$. Experimental results are obtained on samples absorbed in nanoporous matrices or in the form of thin films. We shall not be comprehensive here and will present only a terse overview of the relevant principal findings by DRS measurements. Dynamics of low-molecular-weight molecules confined to nanopores or thin films are usually characterized by broadening of the segmental process, shift of the average relaxation time to higher frequency, and the appearance of an additional (slower) process attributed to interfacial interactions and confinement-induced density inhomogeneities in thin film.[28,30,33,34] In nanopores of 2.5 nm or less, according to Arndt et al.,[35] the segmental process becomes slower than in the bulk liquid, but other studies show that $\alpha$-relaxation does not depend on the pore size and is not affected by the 2D confinement in thin films.[36,37] Studies on the dynamics of polymers confined in nanopores[12,28,34,36] yield results similar to those for low-molecular-weight compounds; segmental and normal processes become broader and, occasionally, an additional intermediate relaxation appears. In thin films of PI, a confinement-induced mode shows up when the film thickness becomes comparable with the average size of the random coil, and it becomes faster with further decrease in thickness.[38] An interesting observation was made in a study of PI confined in glass pores, whereby the normal mode process was found to slow down (slightly) for $M < M_e$ but speed up for $M > M_e$.[30]

Another form of the effect of confinement on dynamics is encountered in polymer blends containing one crystallizable

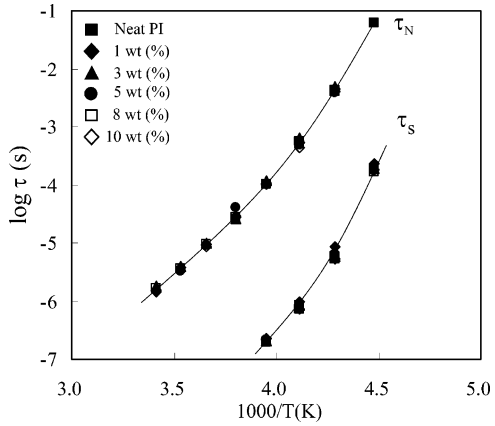


**Figure 7.** Average relaxation time for normal and segmental mode of PI3C25A as a function of reciprocal temperature with clay loading as a parameter. Solid lines are fits to the VFT functional form.

**Table 2. VFT Fit Parameters for Figure 7**

| | mode | | | | | |
|---|---|---|---|---|---|---|
| | normal | | | segmental | | |
| sample | log $\tau_0$ | $T_0$ (K) | $B$ (K) | log $\tau_0$ | $T_0$ (K) | $B$( K) |
| PI3C25A | −9.89 | 165 | 1200 | −9.26 | 195.5 | 350 |
| PI3C30B | −9.9 | 165 | 1197 | −9.3 | 197 | 349 |

component. A study of miscible blends of poly(vinylidene fluoride)/poly(methyl methacrylate) (PVDF/PMMA) by DRS over a wide range of composition, temperature, and frequency showed that the dynamics of the α process in PVDF (crystallizable component) were governed by the physical dimensions of the nanoscopic PVDF regions and by the length scale for cooperative relaxations of PVDF segments.[39] At sufficiently high temperature, the average size of PVDF regions is greater than the length scale for segmental motions, and the most probable relaxation time is independent of blend composition. With decreasing temperature, however, the length scale for segmental motions becomes commensurate with the size of nanoscopic regions, and the relaxation becomes governed by the confinement, which is imposed by the rigid PMMA segments and lamellar PVDF crystals. The effect of confinement increases with decreasing amount of PVDF in the blend, which results in the decrease in the size of PVDF nanoscopic domains. This further leads to a decrease in the average relaxation time for the α process, owing to a preferential suppression of larger scale motions (lower frequency tail of the spectrum) of PVDF segments. A direct consequence of the effect of confinement on dynamics is the crossover from segmental (the α process) to localized motion (the $\beta$ process).

When considering the effect of confinement on relaxation processes in nanocomposites, it is instructive to envision the various scenarios for the inclusion of polymer chains between the silicate layers. In the case of exfoliation, polymer chains diffuse into the gallery and push apart the silicate layers, giving rise to the least confined state. Intercalation is characterized by expansion but not separation of the galleries, and hence a more confined environment is produced. The most confined state is attained when polymer chains diffuse into the galleries without changing the basal spacing. This situation is most likely to restrict chain motions and affect relaxation.

Let us now examine our results. The VFT fits for the temperature dependence of the average relaxation time for normal ($\tau_N$) and segmental ($\tau_S$) mode (obtained from the HN fits) for PI3C25A are shown in Figure 7. The vast majority of the hitherto reported studies[28−39] are concerned with the effect

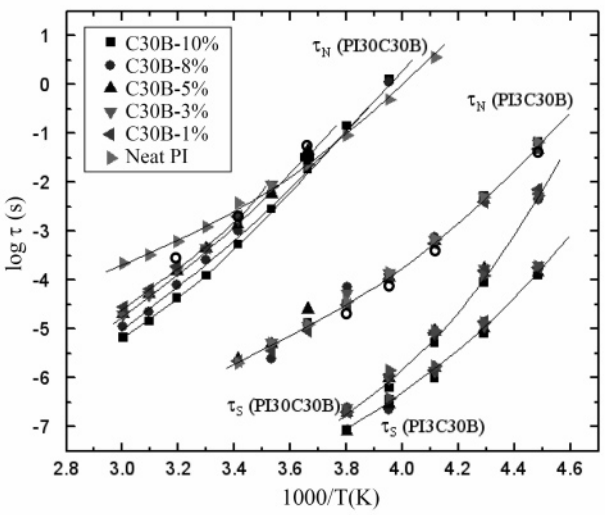


**Figure 8.** Average relaxation time for normal and segmental mode for PI30C30B and PI3C30B nanocomposites at several clay loadings (wt %) as a function of reciprocal temperature. Dynamic mechanical relaxation time (open circle) for PI3C30B5% and PI30C30B5% is shown for comparison.

of confinement on the segmental α process, and we consider that process first. We find no effect on the segmental process of the type and concentration of clay, or the molecular weight of PI within the nonentangled regime, confirming that the time scale and the length scale of the α process are essentially unaffected by the variation in composition and/or molecular architecture. The small difference in the segmental relaxation time for the nonentangled (PI3C30B) and entangled (PI30C30B) PI has been also seen by Imanishi et al., who reported that the segmental process was affected by the MW of PI below a critical value, which in their case was 5000 g/mol.[4] Excellent VFT fits of the segmental process were obtained with the value of $\tau_0$ fixed at the attempt frequency of $10^{-14}$s, as illustrated in Figure 7 and Table 2.

Normal mode process was examined next, starting with PI3 and its nanocomposites. The average relaxation time for the normal mode process in the neat PI3 was unaffected by the addition of clay, as shown in Figure 7. Apparently, the relaxation of the cumulative dipole moment along the chain contour is not affected by confinement because of the low molecular weight of the nonentangled PI3. To establish how the varying length scale of the normal mode process is affected by the confinement, we prepared and tested a nanocomposite consisting of a higher molecular weight PI matrix (PI30, MW = 26.9 kDa) and Cloisite-30B. The results are shown in Figure 8. Most interestingly, we find that the normal mode process becomes faster with increasing clay loading within most of the temperature range investigated. This observation is in contrast with some previous studies on thin films and nanoporous glass that have reported a slower normal mode process in the two-dimensionally confined geometry.[28,29,36,40] But another study found that the normal mode process was not affected in thin films, even when the thickness was smaller than the end-to-end distance.[27] It is our opinion that those different findings are not a priori contradictory because the normal mode process may be affected by a number of variables that include the experimental conditions, type of confinement, extent of intercalation/exfoliation, surface properties, and interfacial interactions. A possible explanation for our findings lies in the preferential suppression of the longer scale (lower frequency) portion of the normal mode process. To account for the faster

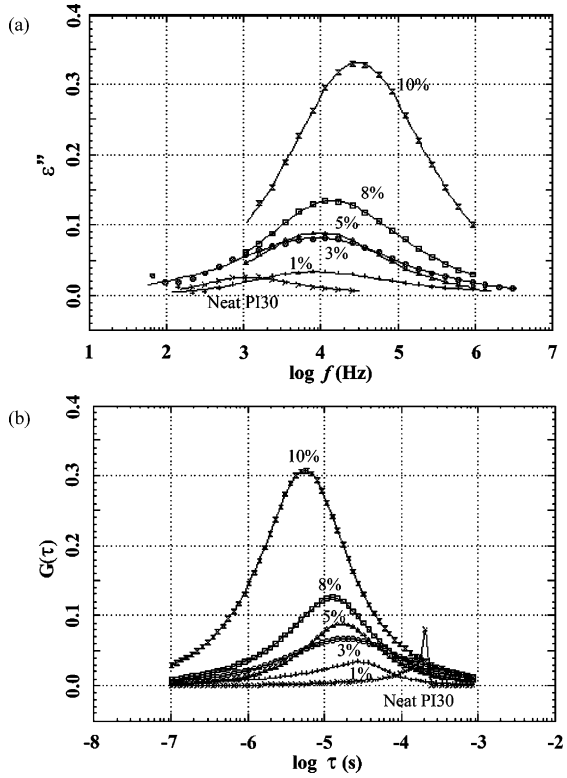


**Figure 9.** (a) Dielectric loss in the frequency domain and (b) relaxation time distribution for PI30C30B with clay loading as a parameter at $T = 323$ K.

normal mode relaxation with increasing clay loading, we consider the change in the conformation and the end-to-end distance of confined chains. Our XRD results suggest that the intercalation and/or exfoliation decrease with increasing clay loading due to the lower number density of PI chains. The implication is that an increasing number of layered silicates accommodate PI chains in the galleries without expanding the basal spacing, resulting in the confined chains that are "squeezed" and the end-to-end distance that is increased. This picture is in agreement with Petychakis et al.,[30] who reported faster normal mode relaxation in a high molecular weight PI confined in glass pores and explained their results in terms of the competition between chain segments for the same portion of glass surface. They argue that this competition creates "dynamic stickers" within the pores that leave only the chain ends uninfluenced by the confinement, resulting in faster relaxation due to shorter chain length. An analogous scenario is envisioned in the nanocomposites used in this study. That, in turn, would induce a shift of the normal mode spectrum toward higher frequency, resulting in (apparently) faster relaxation. This concept was advanced by Kremer[41] and was later invoked by our group in the study of polymer blend (PVDF/PMMA) dynamics that was described earlier in the text.[39]

The average relaxation time for PI3C30B(5%) and PI30C30B-(5%) obtained from the H−N fits of the DMS master curves is also included in Figure 8 for comparison. The results show an excellent agreement between DRS and DMS data for both low (PI3C30B) and high MW (PI30C30B) nanocomposites. Rheological data for the low molecular weight nanocomposites (PI3C30B) are discussed in detail later in the text.

Figure 9a shows how the dielectric loss associated with the normal mode process in PI30C30B shifts to higher frequency with increasing clay loading. At the same time, as seen in Figure 9b, the relaxation time distribution, $G(\tau)$, shifts toward shorter times (faster relaxation). The observed shift is accompanied by the broadening of the relaxation spectrum, a manifestation of the effect of confinement on the length scale of the normal mode process.

An examination of Table 3 reveals an increase in the dielectric strength of the normal mode with increasing clay content (regardless of the type of clay). On the basis of the Onsager-type equations, the relaxation strength is proportional to the mean-squared end-to-end distance and the dipolar moment per contour length unit. The chains that enter the silicate galleries but do not alter their basal spacing will inevitably undergo a conformational change, and the ensuing increase in the end-to-end distance would account for the observed increase in the dielectric strength. An increase in the number density of chains confined in nonintercalated and/or nonexfoliated galleries with clay content explains the systematic increase in the dielectric strength seen in Table 3. The faster normal mode process, on the other hand, is principally due to the shorter effective length scale over which relaxation takes place.

**Dynamic Mechanical Spectroscopy (DMS).** *Effect of Clay Loading and Temperature.* The results of dynamic mechanical spectroscopy (DMS) are considered next. Storage modulus ($G'$) and loss modulus ($G''$) in the frequency domain are shown in parts a and b of Figure 10, respectively, for a series of clay

**Table 3. Dielectric Strength of the Normal Mode Process for (a) PI30C30B and (b) PI30C25A Nanocomposite as a Function of Temperature and Clay Loading Obtained from the H−N Fits**

(a) PI30C30B

| clay (C30B) loading (%) | temp (K) 333 | 323 | 313 | 303 | 293 | 283 | 273 | 263 |
|---|---|---|---|---|---|---|---|---|
| neat PI | 0.12 | 0.12 | 0.12 | 0.12 | 0.12 | 0.14 | 0.14 | 0.14 |
| 1 | 0.24 | 0.23 | 0.21 | 0.21 | 0.17 | 0.16 | 0.17 | 0.11 |
| 3 | 0.50 | 0.46 | 0.48 | 0.45 | 0.45 | 0.45 | 0.37 | 0.31 |
| 5 | 0.71 | 0.69 | 0.68 | 0.62 | 0.63 | 0.57 | 0.50 | 0.41 |
| 8 | 0.87 | 0.78 | 0.78 | 0.75 | 0.75 | 0.72 | 0.68 | |
| 10 | 2.00 | 2.00 | 2.10 | 2.10 | 2.20 | 2.30 | | |

(b) PI30C25A

| clay (C25A) loading (%) | temp (K) 333 | 323 | 313 | 303 | 293 | 283 | 273 | 263 |
|---|---|---|---|---|---|---|---|---|
| neat PI | 0.12 | 0.12 | 0.12 | 0.12 | 0.12 | 0.14 | 0.14 | 0.14 |
| 1 | 0.23 | 0.23 | 0.22 | 0.20 | 0.17 | 0.15 | 0.14 | 0.14 |
| 3 | 1.35 | 1.35 | 1.35 | 1.26 | 1.10 | 0.98 | | |
| 5 | 1.85 | 1.85 | 1.88 | 1.95 | 1.92 | 1.92 | | |
| 8 | 1.5 | 1.50 | 1.57 | 2.00 | 2.05 | 2.70 | | |
| 10 | 2.1 | 2.40 | 2.70 | 2.90 | 2.90 | 2.90 | | |

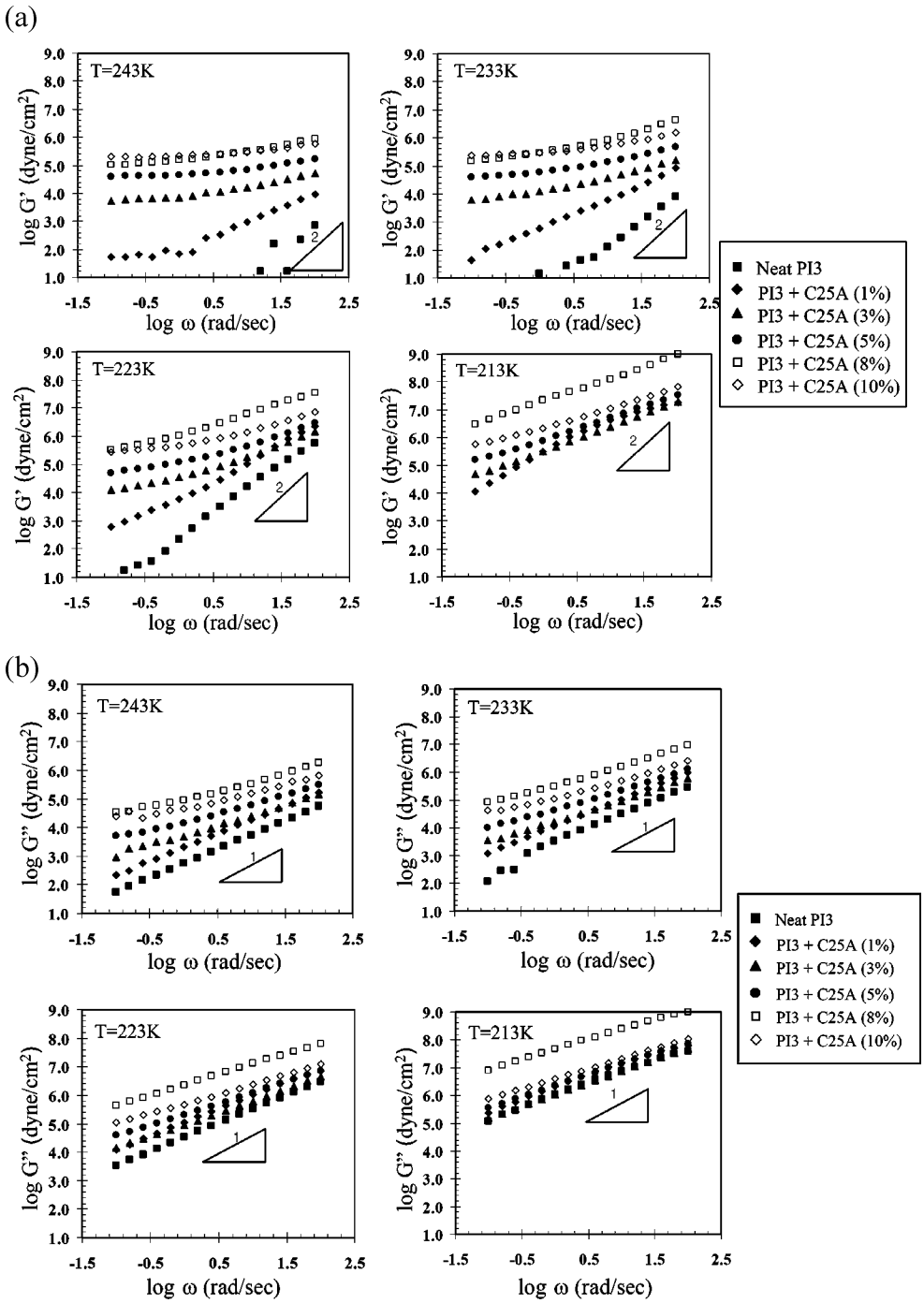


**Figure 10.** (a) Dynamic storage modulus ($G'$) and (b) dynamic loss modulus ($G''$) of PI3 nanocomposites in the frequency domain at different temperature and clay loading.

loadings and temperatures. Neat PI3 exhibits the characteristic response of a linear viscoelastic polymer in the terminal relaxation zone where $G'$ and $G''$ scale with frequency to the power of 2 and 1, respectively. The addition of clay shifts the $G'$ and $G''$ curves upward and leads to a pronounced deviation from the terminal behavior that is particularly noticeable at the low-frequency end of the spectrum. Both $G'$ and $G''$ increase gradually with clay loading before reaching a threshold value at about 10%. The observed increase in $G'$ and $G''$ of about 3 orders of magnitude at the highest clay loading is indicative of the interactions between polyisoprene and dispersed layered silicates through geometric percolation.[9,42] In the low-frequency range, all samples with ≥5% clay are characterized by a frequency-independent storage modulus; with increasing clay loading this frequency-independent region becomes broader. The effect of clay loading on the dynamic moduli becomes comparatively smaller as the temperature is decreased from 243 to 213 K. Interestingly, the storage and loss modulus for 8% clay loading are higher than those for other clay loadings at $T =$ 213 K, suggesting a maximum percolation.

Low-molecular-weight PI3/silicate nanocomposites do not show change in the average relaxation time for the normal mode process but exhibit a notable increase in the dynamic modulus. The unchanged relaxation rate is readily rationalized from the length scale point of view. PI3 chains are characterized by a short length scale ($R_g$ is around 1.6 nm) that does not impair their mobility inside the galleries (intercalated or not) and is not conducive to entanglement traps on the filler surface. These

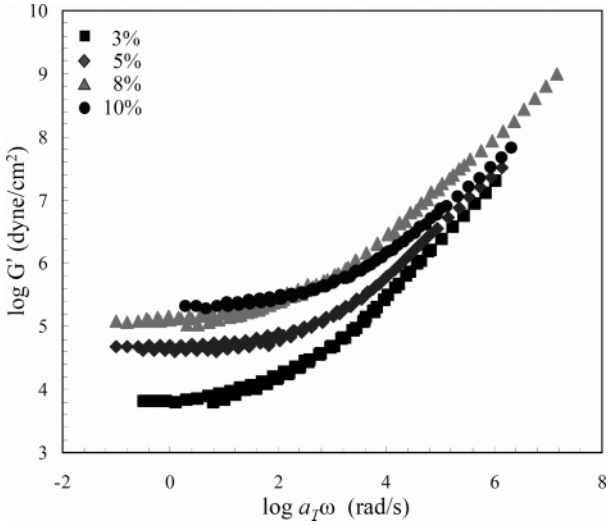


**Figure 11.** Time−temperature superposed dynamic storage modulus for PI3C25A with clay loading as a parameter at $T_0 = 263$ K.

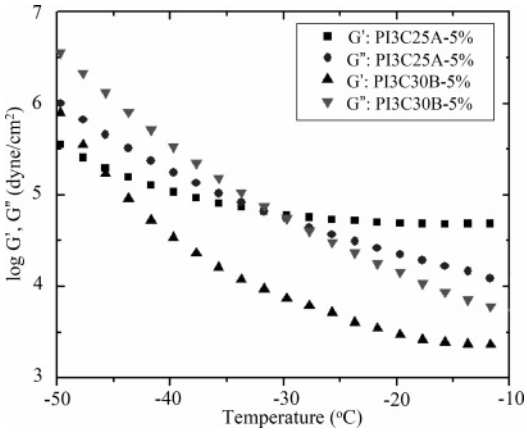


**Figure 12.** Dynamic storage and loss moduli of PI3C25A(5%) and PI3C30B(5%) as a function of temperature at $\omega = 10$ rad/s.

DMS results are consistent with the DRS data, where no shifts of normal or segmental modes are observed with varying clay loading. The average relaxation times for two nanocomposites obtained from the HN fits of the DMS data are included in Figure 8 for comparison. The observed increase in the dynamic moduli, $G'$ and $G''$, in PI3−silicate nanocomposites originates from the "filler effect"—due to the layered silicates dispersed in the PI matrix. This filler effect is commonly evidenced as the increase in stiffness with increasing clay loading, resulting in higher storage than loss modulus. The type of clay also influences the dynamic moduli since the interactions between PI and clay affect the dispersion of filler and the level of reinforcement. The filler effect in PI3−silicate nanocomposites as manifest in the $G'$ vs $G''$ plane is discussed in the latter part of this article.

Figure 11 depicts the time−temperature superposed master curves for storage modulus of PI3C25A with clay loading as a parameter. The master curves were constructed using only the horizontal shift factor $a_T$. The frequency-independent storage modulus, readily observed in the reduced frequency domain, increases with increasing clay loading and reaches a threshold value at 8%. A comparison of the storage and loss moduli for two nanocomposites with the same percentage but different type of clay is shown in Figure 12. Within the temperature range tested, the storage modulus is higher for PI3C25A(5%) than PI3C30B(5%), at least partly due to the enhanced compatibility between the PI matrix and C25A. The effect of the type of filler on dynamic modulus is discussed in more detail below. The pseudo-solid-like, frequency-independent behavior in the low-frequency region of Figure 11 is attributed to the filler effect resulting from the percolation network of nanosilicate platelets in the PI matrix. This is further supported by the fact that $G'$ does not exceed $G''$ by orders of magnitude as is common in solids.[9,43,44] At higher frequencies, $G'$ and $G''$ show the same trend irrespective of temperature, though $G'$ is more sensitive than $G''$.

*Comparison of Dielectric (DRS) and Viscoelastic (DMS) Relaxations.* We next address the question of how dielectric and viscoelastic relaxation are related in nanocomposites as a function of the type of clay and the molecular weight of PI. We consider the low-molecular-weight PI nanocomposites first. Time−temperature superposed storage modulus, loss modulus, and tan $\delta$ for PI3C30B(3%) are displayed as a function of reduced frequency in Figure 13a. The loss modulus data, replotted in Figure 13b, are deconvoluted into normal and segmental processes centered around $10^4$ and $10^7$ rad/s, respectively. Deconvolution was carried out using the HN functional form. The HN fits of the DRS spectra of the same sample at the same temperature are shown in Figure 13c, affording a direct comparison of dielectric and viscoelastic response. The average relaxation time for the normal mode ($\tau_N$) and the segmental mode ($\tau_S$) calculated from the DRS and DMS spectra are in good agreement and are included in Figure 8. Next, the same analysis was applied to a nanocomposite with the higher molecular weight matrix (PI30) and different clay (C25A). Figure 14 illustrates the normal mode process in PI30C25A-(3%) at 313 K, as described by dynamic mechanical loss modulus (a) and dielectric loss (b). Note that the DRS and DMS results are again in excellent agreement.

*Thermorheological Simplicity/Complexity.* We next address the question of thermorheological simplicity/complexity using the log $G'$−log $G''$ protocol utilized by Han and Lem.[45,46] This concept has been used in the studies of morphology and viscoelasticity of thermotropic liquid-crystalline polymers, polymer blends, and filled polymers. Of interest in this work is to inspect the thermorheological simplicity/complexity in nanocomposites that have (1) the same type and amount of clay but varying molecular weight PI and (2) a different type of clay but the same molecular weight PI. In Figure 15 we show a $G'$−$G''$ plot in the temperature range from 213 to 313 K for two nanocomposites with the same clay loading but a different molecular weight PI (PI3 and PI30). Over the range studied, the $G'$−$G''$ plots for both PI3C25A(5%) and PI30C25A(5%) are largely temperature independent and hence thermorheologically simple. At the low-temperature end of the plot, the nanocomposite with lower molecular weight PI (PI3C25A(5%)) has a higher storage modulus, suggesting that percolation is facilitated by the low-molecular-weight matrix. The effect of the type of clay is considered next. Figure 16 provides a comparison of the $G'$−$G''$ plots for two nanocomposites with PI3 matrix but different clay particles (C25A vs C30B) at the same loading (5%). Apart from the minor scatter in the low-temperature range, both samples are again thermorheologically simple. The higher value of $G'$ seen in PI3C25A(5%) is interpreted as the signature of better compatibility of PI with C25A than C30B.

*Effect of Type of Clay on Apparent Activation Energy.* Next, we determine the WLF shift factor, plot it as a function of reciprocal temperature, and calculate the apparent activation

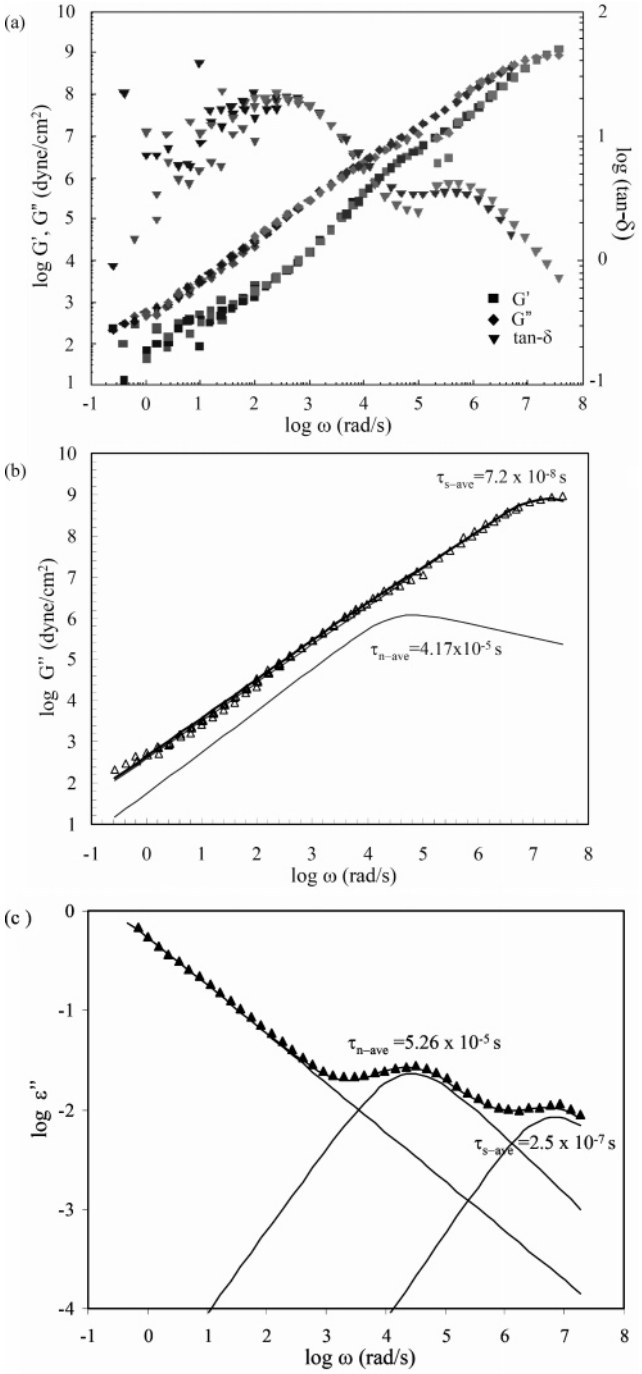


**Figure 13.** (a) Time−temperature superposed storage modulus, loss modulus, and tan $\delta$, (b) deconvoluted loss modulus master curve, and (c) HN fit of dielectric loss for PI3C30B(3%) at $T = 263$ K.

energy in our systems using the following equation:[47,48]

$$E_a = R\left(\frac{\mathrm{d}\ln a_T}{\mathrm{d}(1/T)}\right) = 2.303R\left[\frac{C_1C_2T^2}{(C_2 + T - T_0)^2}\right] \qquad (3)$$

where $C_1$ and $C_2$ are constants and $T_0$ is the reference temperature (in this case 303 K).

The horizontal shift factor ($a_T$) and the apparent activation energy are displayed in Figure 17 and Table 4 as a function of clay loading and temperature. The $a_T$ factor depends on the clay content, and hence the activation energy may be considered as an indicator of the molecular mobility and the energy barrier that must be overcome as nanoclay particles percolate in the PI

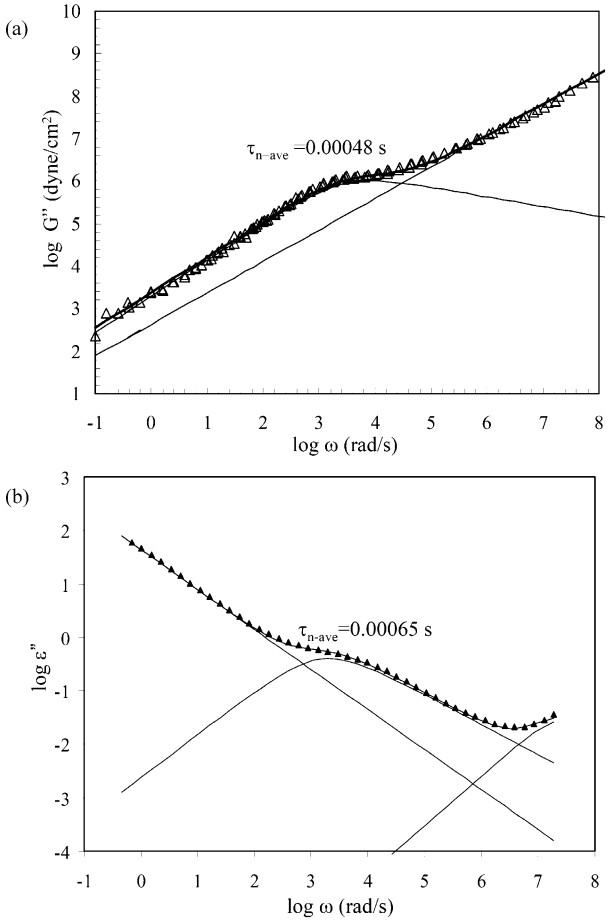


**Figure 14.** (a) HN fit of the time−temperature superposed dynamic loss modulus and (b) HN fit of the dielectric loss for PI30C25A(3%) at $T = 313$ K.

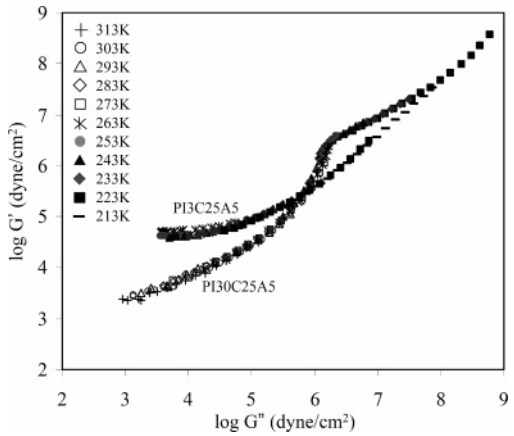


**Figure 15.** Dynamic storage modulus vs loss modulus for PI3C25A-(5%) and PI30C25A(5%) at various temperatures.

matrix. The principal difference between the C30B and C25A is that the former is polar and has a smaller basal spacing. The question is if and how that difference affects the mobility of PI chains confined in the galleries. Our calculations, summarized in Table 4, yield lower activation energy in C25A (nonpolar) than in C30B (polar) nanocomposites. The lower activation energy in the PI3C25A nanocomposites is due to the initially larger gallery height in C25A and the similar chemical structure of C25A and PI (both nonpolar). As a result, the PI chains penetrate more readily into the gallery of silicate layers, resulting in an enhanced capability for exfoliation or intercalation. The

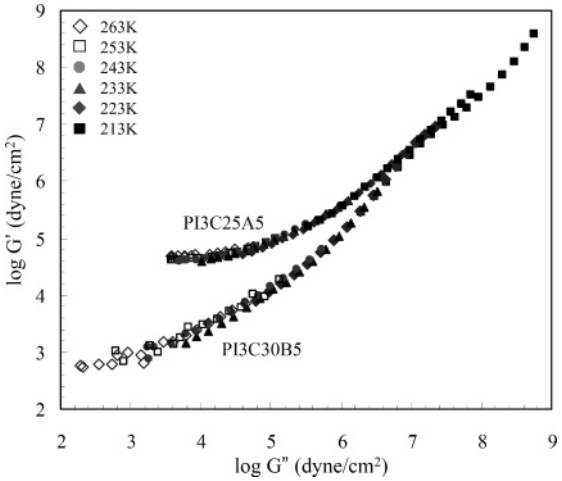


**Figure 16.** Dynamic storage modulus vs loss modulus for PI3C30B-(5%) and PI3C25A(5%) at various temperatures.

apparent activation energy increases with increasing clay content, peaks at 8% loading, and then decreases at 10% for both PI3C25A and PI3C30B.

## Conclusions

We have completed an investigation of the dynamics of nanocomposites of layered silicate nanoparticles and *cis*-polyisoprene (PI) matrix. Two different types of organically modified clay and two different molecular weight PI homopolymers (in entangled and nonentangled regimes) were used to prepare the samples. The extent of intercalation and/or exfoliation was determined by X-ray diffraction measurements and was found to vary with the amount and type of clay. Dynamics

**Table 4. Activation Energy[a] Calculated from Eq 3 for (a) PI3C25A and (b) PI3C30B**

(a) PI3C25A

| | temp (K) | | | | | | | |
|---|---|---|---|---|---|---|---|---|
| clay loading (%) | 213 | 223 | 233 | 243 | 253 | 263 | C1 | C2 |
| 1 | 135.7 | 109.9 | 92.3 | 79.6 | | | 6.43 | 91.34 |
| 3 | 113.0 | 96.1 | 83.8 | 74.5 | 67.2 | 61.4 | 5.75 | 124.02 |
| 5 | 138.5 | 107.9 | 88.1 | 74.3 | 64.3 | 56.8 | 4.45 | 103.85 |
| 8 | 174.4 | 134.3 | 108.6 | 91.0 | 78.3 | 68.8 | 5.29 | 101.77 |
| 10 | 169.6 | 125.6 | 98.8 | 81.1 | 68.7 | 59.6 | 4.33 | 96.19 |

(b) PI3C30B

| | temp (K) | | | | | | | |
|---|---|---|---|---|---|---|---|---|
| clay loading (%) | 213 | 223 | 233 | 243 | 253 | 263 | C1 | C2 |
| 1 | 155.7 | 123.5 | 102.0 | 86.9 | | | 6.67 | 86.87 |
| 3 | 192.6 | 131.6 | 98.0 | 77.4 | 63.6 | | 4.02 | 77.50 |
| 5 | 156.4 | 122.3 | 100.0 | 84.5 | 73.2 | 64.7 | 5.10 | 104.33 |
| 8 | 166.3 | 129.1 | 105.1 | 88.5 | 76.4 | 67.4 | 5.25 | 103.20 |
| 10 | 129.6 | 107.4 | 91.7 | 80.2 | 71.3 | 64.4 | 5.67 | 116.56 |

[a] $E_a = R[(\mathrm{d} \ln a_T)/\mathrm{d}(1/T)] = 2.30R[C_1C_2T^2/(C_2 + T - T_0)^2]$.

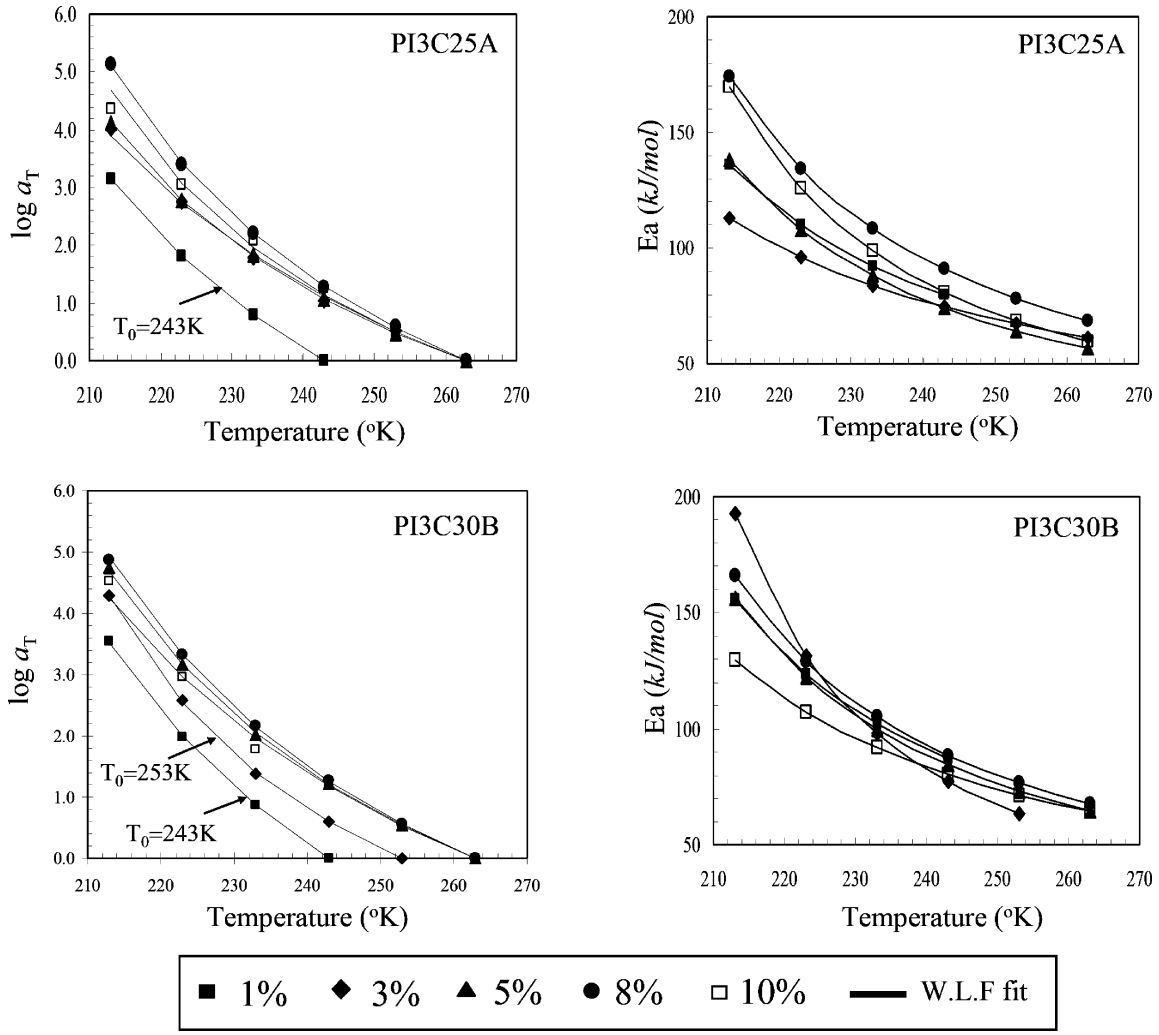


**Figure 17.** Temperature dependence of the horizontal shift factor $a_T$ and apparent activation energy for PI3C25A and PI3C30B with variable clay loading at $T = 263$ K.

of nanocomposites were investigated over a broad range of frequency and temperature using dielectric relaxation spectroscopy (DRS) and dynamic mechanical spectroscopy (DMS). Insertion of PI chains between intercalated or exfoliated clay platelets raises the question of how the restricted space, or confinement, affects the segmental and normal mode processes. We find no effect on the segmental process exerted by the type of clay, the concentration of clay, or the molecular weight of PI within the nonentangled regime, confirming that the time scale and the length scale of the α process are essentially not affected by the variation in composition and/or molecular architecture. However, a clear effect of clay loading on the dc conductivity and the interfacial polarization was observed. Nanocomposites with the high-molecular-weight ($M > M_e$) PI matrix were characterized by a decrease in the average relaxation time for the dielectric normal mode with increasing clay loading. This interesting finding is interpreted as the effect of confinement that is manifest through the preferential suppression of the longer scale (lower frequency) portion of the normal mode spectrum. This can be further rationalized by considering the change in the conformation and the end-to-end distance of PI chains that are accommodated within the silicate galleries. A direct comparison of DRS and DMS results, made by deconvolution of dielectric and viscoelastic spectra, showed excellent agreement between the average relaxation time for both segmental and normal mode relaxation. Addition of clay increases the storage ($G'$) and loss modulus ($G''$) and leads to a pronounced deviation from the terminal behavior. Both $G'$ and $G''$ increase gradually with clay loading before reaching a threshold value at about 10%. In the low-frequency range, all samples with ≥5% clay are characterized by a frequency-independent storage modulus. The observed increase in $G'$ and $G''$ is attributed to the "filler effect" and is indicative of the interactions between the dispersed layered silicates and the PI matrix through geometric percolation.

**Acknowledgment.** This material is based on work supported by National Science Foundation under Grant DMR-0346435. We thank Professor E. J. Donahue of the Long Island University for generous help with the XRD measurements.

## References and Notes

(1) Jeon, H. S.; Rameshwaram, J. K.; Kim, G.; Weinkauf, D. H. *Polymer* **2003**, *44*, 5749.
(2) Peanasky, J.; Cai, L. L.; Granick, S. *Langmuir* **1994**, *10*, 3874.
(3) Anastasiadis, S. H.; Karatasos, K.; Vlachos, G. *Phys. Rev. Lett.* **2000**, *84*, 915.
(4) Imanishi, Y.; Adachi, K.; Kotaka, T. *J. Chem. Phys.* **1988**, *89*, 7585.
(5) Boese, D.; Kremer, F. *Macromolecules* **1990**, *23*, 829.
(6) Yoshida, H.; Adachi, K.; Watanabe, H.; Kotaka, T. *Polym. J.* **1989**, *21*, 863.
(7) Watanabe, H.; Matsumiya, Y.; Inoue, T. *Macromol. Symp.* **2005**, *228*, 51.
(8) Ren, J.; Silva, A. S.; Krishnamoorti, R. *Macromolecules* **2000**, *33*, 3739.
(9) Jeon, H. S.; Rameshwaram, J. K.; Kim, G. *J. Polym. Sci., Part B: Polym. Phys.* **2004**, *42*, 1000.
(10) Vu, Y. T.; Mark, J. E.; Pham, L. H.; Engelhardt, M. *J. Appl. Polym. Sci.* **2001**, *82*, 1391.
(11) Kobuke, Y.; Fueno, T.; Furukawa, J. *J. Polym. Sci.* **1970**, *8*, 2979.
(12) Kremer, F.; Schonhals, A. *Broadband Dielectric Spectroscopy*; Springer-Verlag: Berlin, 2003.
(13) Mijovic, J.; Kenny, J. M.; Maffezzoli, A.; Trivisano, A.; Belluccci, F.; Nicolais, L. *Compos. Sci. Technol.* **1993**, *49*, 277.
(14) Mijovic, J.; Sy, J. W. *Macromolecules* **2000**, *33*, 9620.
(15) Riande, E., Calleja, R. D., Eds.; *Electrical Properties of Polymers;* Marcel Dekker: New York, 2004.
(16) Angell, C. A.; Ngai, K. L.; McKenna, G. B.; McMillan, P. F.; Martin, S. W. *J. Appl. Phys.* **2000**, *88*, 3113.
(17) Watanabe, H.; Matsumiya, Y.; Osaki, K. *J. Polym. Sci., Part B: Polym. Phys.* **2000**, *38*, 1024.
(18) Neagu, R. M.; Neagu, E.; Bonanos, N.; Pissis, P. *J. Appl. Phys.* **2000**, *88*, 6669.
(19) Steeman, P. A. M.; Maurer, F. H. J.; Turnhout, J. V. *Polym. Eng. Sci.* **1994**, *34*, 697.
(20) Wubbenhorst, M.; Koten, E. M. V.; Jansen, J. C.; Mijs, W.; Turnhout, J. V. *Macromol. Rapid Commun.* **1997**, *18*, 139.
(21) Steeman, P. A. M.; Gondard, C.; Scherrenberg, R. L. *J. Polym. Sci., Part B: Polym. Phys.* **1994**, *32*, 119.
(22) Kalogeras, I. M.; Neagu, E. K. *Eur. Phys. J. E* **2004**, *14*, 193.
(23) Ray, S. S.; Okamoto, K.; Okamoto, M. *Macromolecules* **2003**, *36*, 2355.
(24) Mitchell, C. A.; Krishnamoorti, R. *J. Polym. Sci., Part B: Polym. Phys.* **2002**, *40*, 1434.
(25) Kanapitsas, A.; Pissis, P.; Kotsilkova, R. *J. Non-Cryst. Solids* **2002**, *305*, 204.
(26) Pissis, P.; Kyritsis, A. *Solid State Ionics* **1997**, *97*, 105.
(27) Georgoussis, G.; Kanapitsas, A.; Pissis, P.; Savelyev, Y. V.; Veselov, V. Y. *Eur. Polym. J.* **2000**, *36*, 1113.
(28) Schonhals, A.; Stauga, R. *J. Chem. Phys.* **1998**, *108*, 5130.
(29) Aoyagi, T.; Takimoto, J.; Doi, M. *J. Chem. Phys.* **2001**, *115*, 552.
(30) Petychakis, L.; Floudas, L.; Fleischer, G. *Europhys. Lett.* **1997**, *40*, 685.
(31) Jackson, C. L.; McKenna, G. B. *J. Chem. Phys.* **1990**, *93*, 9002.
(32) Jackson, C. L.; McKenna, G. B. *J. Non-Cryst. Solids* **1991**, 221.
(33) Ngai, K. L. *Eur. Phys. J. E* **2002**, *8*, 225.
(34) Manias, E.; Kuppa, V. *Eur. Phys. J. E* **2002**, *8*, 193.
(35) Arndt, M.; Stannarius, R.; Groothues, H.; Hempel, E.; Kremer, F. *Phys. Rev. Lett.* **1997**, *79*, 2077.
(36) Swenson, J.; Schwartz, G. A.; Bergman, R.; Howells, W. S. *Eur. Phys. J. E* **2003**, *12*, 179.
(37) Schonhals, A.; Goering, H.; Schick, Ch.; Frick, B.; Zorn, R. *Eur. Phys. J. E* **2003**, *12*, 173.
(38) Serghei, A.; Kremer, F.; Kob, W. *Eur. Phys. J. E* **2003**, *12*, 143.
(39) Sy, J. W.; Mijovic, J. *Macromolecules* **2000**, *33*, 933.
(40) Cho, Y. K.; Watanabe, H.; Granick, S. *J. Chem. Phys.* **1999**, *110*, 9688.
(41) Kremer, F.; Hartmann, L.; Serghei, A.; Pouret, P.; Leger, L. *Eur. Phys. J. E* **2003**, *12*, 139.
(42) Li, J.; Zhou, C.; Wang, G.; Zhao, D. *J. Appl. Polym. Sci.* **2003**, *89*, 3609.
(43) Kim, K. N.; Kim, H.; Lee, J. W. *Polym. Eng. Sci.* **2001**, *41*, 1963.
(44) Krishnamoorti, R.; Giannelis, E. P. *Macromolecules* **1997**, *30*, 4097.
(45) Zarraga, A.; Pena, J. J.; Munoz, M. E.; Santamaria, A. *J. Polym. Sci., Part B: Polym. Phys.* **2000**, *38*, 469.
(46) Han, C. D.; Lem, K. *Polym. Eng. Rev.* **1982**, 135.
(47) Ferry, J. D. *Viscoelastic Properties of Polymers*; John Wiley & Sons: New York, 1980.
(48) Kwak, S. Y.; Oh, K. S. *Macromol. Mater. Eng.* **2003**, *288*, 503.

MA051995E